scientific reports

OPEN

Effect of acid proticity on the thermodynamic parameters of charge transfer resistance in corrosion and passivation of nickel based glass alloy

Khadijah M. Emran[1]✉ & Noureddine Ouerfelli[2]

The effect of temperature on electrochemical properties of $Ni_{82.3}Cr_7Fe_3Si_{4.5}B_{3.2}$ glassy alloy in different acid proticity has been investigated utilizing AC and DC methods. Firstly, the handling of experimental data on the temperature dependence of charge transfer resistance, as well as corrosion current density permits us to determine the values of classical Arrhenius parameters as well as the thermodynamic ones considered approximately independent of temperature. This leads us to deduce a global interpretation on the phenomenon of corrosion and polarization. Secondly, the deviation to the linearity of the Arrhenius behavior and the real dependence on temperature of the thermodynamic parameters, permit us to clearly quantify the effect of the acid proticity and define, for the first time, the concept of current Arrhenius parameters and the current thermodynamic ones, as well as the modeling of the enthalpy–enthalpy compensation. Moreover, the effect of temperature can be investigated using the Vogel–Fulcher–Tammann model to reveal that the corresponding Vogel temperature has an interesting physical meaning.

The high corrosion resistance features that often extend an improved corrosion resistance of metallic glasses which chemically afford a smooth contacting metallic surface with minimal defects and free of voids, dislocations and/or atomic terraces, so they have no crystallographic dislocations, crystal imperfections, distortions, grain boundaries or secondary phase elements[1–3]. Passivation is the process of making a material "non-reactive" in relation to another material[4,5]. After corrosion process, passivation is the spontaneous formation of a hard non-reactive surface film that inhibits the corrosion process.

High temperature corrosion plays an increasingly important role in the selection of materials, in particular within the power generation industry. The most influencing factors on susceptibility to corrosion of metallic glasses are the nature of the components and high temperatures, either in acidic or alkaline media[6–10].

For nickel-contained glassy alloys, the effects of microstructure change on the corrosion behaviors of $Ni_{55}Nb_{20}Ti_{10}Zr_8Co_7$ glassy alloy were investigated in 1 mol/L HCl and 0.5 mol/L H_2SO_4 solutions[11]. Anodic polarizations, at range 872 K to 1050 K, reveal the high corrosion resistance for all the alloys, which can be due to the formation of a passive film on the alloy surface corrosion behavior of $Al_{86}Ni_{10}Y_4$ and $Al_{83}Ni_{13}Y_4$ amorphous alloys which was investigated in 3.5 *wt*.% NaCl solution[12]. The electrochemical techniques reveal the rapidly solidified $Al_{86}Ni_{10}Y_4$ and $Al_{83}Ni_{13}Y_4$ alloys which exhibit better passivity and higher polarization resistance after annealing at 150 °C.

The effects of Mo and Cr substitution for Ni on $Ni_{77-x-y}Mo_xCr_yNb_3P_{14}B_6$ ($x = 5$–9, $y = 0$–5) glassy alloy corrosion have been studied in 1 M NaCl and 1 M HCl solutions. The addition of the appropriate Mo and Cr content as much as possible are beneficial for the enhancement of the corrosion resistance of the present Ni-based (bulk metallic glasses) BMGs with an I_{corr} in the order of 10^{-6} A/cm^2 and a R_{corr} about 10^{-3} mm/year in both solutions[13].

In a recent research, Han et al.[14] studied the high temperature oxidation behaviors for $Ir_{35}Ni_{25}Ta_{40}$ and $Ir_{35}Ni_{20}Ta_{40}B_5$ (*wt*%) metallic glasses that become the optimal candidates for the molding materials of optical devices. It was found that Ir–Ni–Ta-(B) MGs display good oxidation resistance and there appears a unique

[1]Chemistry Department, college of Science, Taibah University, Medina, Saudi Arabia. [2]Institut Supérieur des Technologies Médicales de Tunis, LR13SE07, Laboratoire de Biophysique et Technologies Médicales, Université de Tunis El Manar, Tunis, Tunisia. ✉email: kabdalsamad@taibahu.edu.sa

four-layer oxide micro-structure on the surface and the natural oxide Ta_2O_5 will be transformed into TaO_2 with the gradual increase of temperature after approaching T_g of Ir–Ni–Ta-(B) MGs[14]. In another study, the corrosion behavior of $Ni_{62}Nb_{33}Zr_5$ bulk metallic glasses (BMGs) after annealing treatment (AT) at different crystallization temperatures and cryogenic treatment (CT) at –100 °C are experimentally investigated[15]. Superior corrosion resistance is obtained in the cryo-treated BMG because of the high degree of amorphization. The passive film is found to be composed mainly of Nb_2O_5 and ZrO_2, demonstrating that Nb and Zr are conducive to reacting with oxygen to form a passive film. Globally, several recent works treated different conductive and corrosion behaviors in some BMGs materials[16–21].

In our previous study, a systematic study of the corrosion and passivation behavior of the $Ni_{82.3}Cr_7Fe_3Si_{4.5}B_{3.2}$ (*wt%*) in 3.0 mol/L aqueous solutions of HCl, H_2SO_4, and H_3PO_4 acids solutions at temperatures range (20–80) was carried. The passive film on $Ni_{82.3}Cr_7Fe_3Si_{4.5}B_{3.2}$ (*wt%*) glassy alloy surfaces was a uniform and stable chromium oxy-hydroxide [$CrO_x(OH)_{3-2x}\cdot nH_2O$], which is a few atoms thick[1]. In recent research[22] we have extended the Arrhenius-type expression by one term in $1/T^2$ and collected some physical meaning to the new related coefficients for which it is found that they depend closely on the number of acid hydrogen atoms in the polyacid for the corrosion and passivation of the nickel based metallic glass alloy of the composition $Ni_{82.3}Cr_7Fe_3Si_{4.5}B_{3.2}$. We have suggested a mathematical formula that allows indirect calculation of the familiar Arrhenius activation energy using only the parameters of the homographic model for each acid separately or for all three polyacids together.

As a continuation of our previous works[1,22] and, based on the above considerations, we suggest some novel empirical models for thermodynamic parameters in the present work. Therefore, we will introduce a new concept of current quantities after considering the dependence with temperature of the Arrhenius and thermodynamic parameters. Moreover, the novel application of the Vogel–Fulcher–Tammann (VTF) model[14,23–28] on corrosion reveals new physical meanings of the corresponding parameters. Also, the effect of the proton numbers, of the used polyacids, on the thermodynamic parameters is modeled with logarithm form.

Materials and methods

Ni-based alloy ingots $Ni_{82.3}Cr_7Fe_3Si_{4.5}B_{3.2}$ (*wt%*) alloy was prepared by rapid solidification supplied as ribbons of about 2.5–7.5 mm length and 20–50 μm thickness by Vacuumschmelze after polishing operation.

The electrochemical cell included three electrodes such as: the corroded sample as working electrode, a platinum-wire counter electrode and, a saturated calomel reference electrode for which each experiment is realized using a new alloy strip after degreasing in alcohol, rinsing with be-distilled water, and ultrasonic cleaning.

Because of the high aggressivity of acids in the studied temperature range, electrochemical characterization was performed in acidic solutions of 3.0 mol/L of HCl, H_2SO_4, or H_3PO_4 for examining the electrochemical behavior of Ni-based glassy alloy at different temperatures ranging from 20 to 80° before the specimens were destroyed notably at higher temperature.

The electrochemical measurements, on samples with 2 cm^2 surface area, were performed by direct and alternating currents at several temperatures with an ACM Gill AC instrument. Measurements by electrochemical impedance spectroscopy were carried out at frequencies from 0.1 Hz to 30 kHz utilizing sinusoidal wave of 5 mV amplitude. Polarization measurements were realized, at a scan rate of 2 mV/s, from (– 800 to 2000) mV.

Complementary details are presented in our previous works[1,22].

Deviation to Arrhenius behavior

Correlation between Arrhenius parameters

Activation energy control occurs when the electrode kinetics or corrosion rate is controlled by a slow electrochemical step. The activation energy (*Ea*) can be determined from Arrhenius plot that often used to analyze the effect of temperature on the rates of chemical reactions where the reactants molecules colliding probability becomes higher and the reaction proceeds faster at higher temperatures. In our study *Ea* of the corrosion process of glassy alloy in 3.0 mol/L solutions of the studied acids was obtained from the assumed linear variation of the corrosion reaction rate assigned as the reciprocal of the charge transfer resistance, $1/R_{ct}$, with temperature[1,22].

The variation of the charge transfer resistance (R_{ct}) as a function of temperature (T) is considered following the Arrhenius-type equation (Eqs. 1 or 2). In this context, in previous works[1,22] we have applied the Arrhenius-type equation in this exponential and logarithm form where the two Arrhenius parameters are generally supposed both constants practically independent of temperature.

$$R_{ct} = A_{ct} e^{\frac{E_a}{RT}} \tag{1}$$

$$\ln R_{ct} = \ln A_{ct} + \frac{E_a}{R} \times \frac{1}{T} \tag{2}$$

where *Ea* is the activation energy, A_{ct} is the pre-exponential factor (Table 1). Though the theories of collision, transition state, statistical physics, theory or chemical reaction rate have detailed and expressed the effect of temperature, generally[1,22], experimenters assumed that these two Arrhenius parameters are both constants and practically independent of temperature, where the plot of ($\ln R_{ct}$) as a function of the reciprocal of absolute temperature ($1/T$) gives approximately a straight line[1,22] whose the slope is equal to (Ea/R) and the intercept on the ordinate is equal to ($\ln A_{ct}$). Additionally, we can append that in addition to the *y*-intercept ($\ln A_{ct}$) in (Fig. 1 of Ref.[22]), we can also speak of the *x*-intercept ($T_A = -Ea/(R\cdot\ln A_{ct})$) previously named as the Arrhenius temperature[22]. In addition, we have shown that ($-R\cdot\ln A_{ct}$) is considered as an entropic factor (Fig. 3 of Ref.[22]) and closely correlated with the activation entropy ΔS determined from impedance measurements in our earlier work[1] (Table S1).

Acid	E_a/kJ mol^{-1}[1]	$\ln(A_{ct}/\Omega\ cm^2)$[1]	$-R\cdot\ln A_{ct}$/J.K^{-1} mol^{-1}[22]	ΔS/J K^{-1} mol^{-1}[1]*	T_A/K[22]
HCl	52.976	-12.310	102.35	-151.0	517.59
H_2SO_4	83.287	-24.546	204.09	-52.0	408.10
H_3PO_4	102.27	-31.733	263.84	19.0	387.61

Table 1. Arrhenius parameters (Ea and $\ln A_{ct}$), the entropic factor of Arrhenius—$R\cdot\ln(A_{ct})$ from linear regression of Eq. 2, the activation entropy ΔS and Arrhenius temperature (T_A). *Calculated via the variation of the charge transfer resistance ($R_{ct}/\Omega\ cm^2$) as a function of temperature (T).
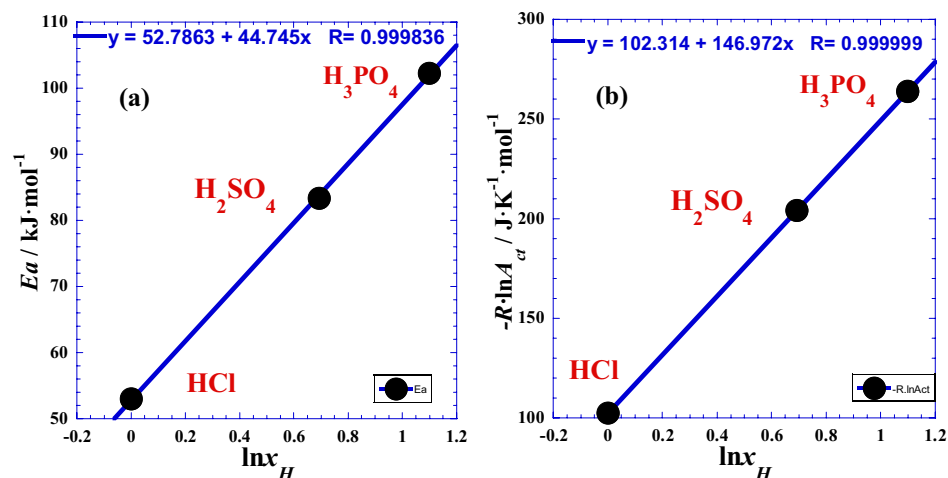

Figure 1. Variation against the logarithm of the acid proticity ($\ln x_H$) of (**a**): the activation energy (Ea) and (**b**): the entropic factor of Arrhenius—$R\cdot\ln(A_{ct})$.

By similarity of some recent studies on the viscosity of liquid state which find that the Arrhenius temperature (T_A) is strongly correlated to the boiling temperature (T_b)[29–31], and regarding that the BMGs are in solid state, we can assume that the Arrhenius temperature (Table 1) is probably in causal correlation with the corresponding glass transition temperature (T_g) which is strongly correlated with the melting point (T_m)[14,26,27]. This allows us in the future to make certain predictions, estimations and comparisons of different BMGs features.

Furthermore, the mutual correlation between the two Arrhenius parameters (Ea and $\ln A_{ct}$) (Table 1), shows quasi-linearity inter-dependence expressed as follows:

$$E_a = E_{a0} + \tau_0 \cdot (-R\ln A_{ct}) \tag{3}$$

where ($E_{a0} = 21.64$ kJ mol^{-1}) is the activation energy corresponding the zero value of the entropic factor, and the slope ($\tau_0 = 304.45$ K) is a temperature characteristic of the studied system at such conditions. Numerical applications require the use of the following convenient simple formulas:

$$E_a(\text{kJ} \cdot \text{mol}^{-1}) = 21.64 - 2.53134 \times \ln\left(A_{ct}/\Omega \cdot cm^2\right)$$

$$\ln\left(A_{ct}/\Omega \cdot cm^2\right) = 8.5488 - 0.39505 \times E_a(\text{kJ} \cdot \text{mol}^{-1})$$

We point out that the values of coefficients can vary according to experimental conditions and to the system characteristics and specificity.

We notice that in the general case when the two Arrhenius parameters (Ea and $\ln A_{ct}$) depend slightly on the temperature, the characteristic temperature (τ_0) becomes the derivative of the activation energy with respect of the entropic factor (Eq. 4) at constant pressure.

$$\tau_0 = -\frac{1}{R}\left(\frac{\partial Ea}{\partial(\ln R_{ct})}\right)_P \tag{4}$$

Since the observed linear dependence between the two Arrhenius parameters Ea and $\ln A_{ct}$ (Eq. 3), the charge transfer resistance R_{ct} can be expressed only against of Ea or $\ln A_{ct}$ (Eqs. 5 and 6), respectively. Indeed, combining (Eqs. 2 and 3) we can write the following expressions:

$$\ln R_{ct} = \frac{E_{a0}}{R\tau_0} + \frac{E_a}{R}\left(\frac{1}{T} - \frac{1}{\tau_0}\right) \tag{5}$$

Or,

$$\ln R_{ct} = \frac{E_{a0}}{RT} + \frac{T - \tau_0}{T} \cdot \ln A_{ct} \tag{6}$$

Numerical applications require the use of the following convenient simple formulas:

$$\ln(R_{ct} / \Omega\mathrm{cm}^2) = 8.5488 + \frac{(E_a/\mathrm{kJmol}^{-1})}{R/1000}\left(\frac{1}{T} - \frac{1}{304.45}\right)$$

$$\ln(R_{ct} / \Omega\mathrm{cm}^2) = \frac{2602.7}{(T/\mathrm{K})} + \frac{T - 304.45}{T} \cdot \ln(A_{ct} / \Omega\mathrm{cm}^2)$$

The values of these coefficients can vary according to experimental conditions and to the characteristics and specificity of the studied system. In addition these two expressions are interesting when only one Arrhenius parameter is predicted by certain theory, the charge transfer resistance R_{ct} can be then estimated by (Eqs. 5 or 6).

To our knowledge, there is no theoretical and physical basis of this observed causal correlation or any developed estimative techniques for our original suppositions. Then, we will be able to give more closely our checking after applying these suggested equations by several researchers in the future.

Based on the studied correlation[26,27] between the glass transition temperature (T_g) and the melting temperature ($T_{m(AxBy)}$) of the base components of various metallic glasses where ($300 \ \mathrm{K} < T_g < 900 \ \mathrm{K}$) and ($600 \ \mathrm{K} < T_{m(AxBy)} < 1600 \ \mathrm{K}$) and the suggested expressions for the viscosity-temperature dependence[29–31], we propose similar predictive expression form for the charge transfer resistance–temperature dependence expressed as follows.

$$\frac{1}{T_A} - \frac{1}{T_m} \approx \frac{1}{T_g} \tag{7}$$

As quick application of this formula, if we take ($T_m = 1726 \ \mathrm{K}$) for some Ni-MGs in (Fig. 1 of Ref.[26]) and the Arrhenius temperature ($T_A = 517.59 \ \mathrm{K}$) in the monoacid medium for our Ni-MG (Table 1), we find, via the (Eq. 7), approximately a value of ($T_g = 739 \ \mathrm{K}$) which is included in the range of the studied set of Ni-MGs in (Fig. 1 of Ref.[26]). We conclude that this approximative estimation can open an interesting path for future investigators to test, valid and improve the proposed model (Eq. 7).

In the same way, by analogy with the viscosity-temperature dependence at liquid phase[29–31] which authors have discovered that the A_{ct} is the pre-exponential factor (Eq. 1) is very close to the viscosity of the same system at vapor phase and at normal boiling temperature, we can presume that our pre-exponential factor (A_{ct}) in (Table 1) probably represents approximately the charge transfer resistance (R_{ct}) in liquid phase at the melting temperature (T_m) or at the glass transition temperature (T_g) under atmospheric pressure.

Effect of protons' number (x_H)

For this query, and to test the effect of number of protons (x_H) of the acids (H_xB), we plotted the two Arrhenius parameters against the logarithm of the acid proticity ($\ln x_H$). Figure 1 shows a spectacular linearity, which leads us to wonder, for future investigations, if this relationship is valid for other strong acids with the same proticity. The slope of the straight line in Fig. 1a represents the activation energy gap ε_g (Table 2) and it corresponds to the jump of energy value when the proticity increases with unity. The same ascertainment is valid for the Fig. 1b concerning the entropic factor gap σ_g (Table 2). This observed linearity can be expressed as follows:

$$E_a(x_H) = E_{a1} + \varepsilon_g \cdot \ln x_H \tag{8}$$

$$-R\ln A_{ct}(x_H) = -R\ln A_{ct1} + \sigma_g \cdot \ln x_H \tag{9}$$

where the straight line parameters are the intercepts on the ordinate (E_{a1}) and ($- R \cdot \ln A_{ct1}$) correspond to the values of the activation energy and entropic factor related to the monoacid HCl ($x_H = 1$), respectively (Table 2). Numerical applications require the use of the following convenient simple formulas:

$$E_a(x_H)/\mathrm{kJ \ mol}^{-1} = 52.976 + 44.745 \cdot \ln x_H$$

$$\ln(A_{ct}(x_H)/\Omega \ \mathrm{cm}^2) = -12.310 - 17.677 \cdot \ln x_H$$

ε_g	E_{a1}	σ_g	$- R \cdot \ln A_{ct1}$
kJ mol^{-1}	kJ mol^{-1}	J.K^{-1} mol^{-1}	J K^{-1} mol^{-1}
44.745	52.786	146.972	102.314
	52.976*		102.35*

Table 2. Straight lines parameters from linear regression of Eqs. 8 and 9. *Correspond to HCl experimental data[1], see Table 1.

The values of these coefficients can vary according to the experimental conditions as well as the system characteristics and specificity.

However, Eqs. 1, 8 and 9 can be re-expressed to explicit the effect of protons number (x_H) of the polyacids (H_xB) based on monoacid HCl ($x_H = 1$) data.

$$A_{ct}(x_H) = A_{ct1} \cdot x_H^{\frac{-\sigma_g}{R}} \tag{10}$$

$$R_{ct}(x_H) = R_{ct1}(T) \cdot x_H^{\frac{\gamma_g}{RT}} \tag{11}$$

$$\gamma_g = \varepsilon_g - T \cdot \sigma_g \tag{12}$$

where γ_g represents a kind of free energy gap of acid protonation, $R_{ct1}(T)$ is the charge transfer resistance related to the monoacid HCl ($x_H = 1$) at given temperature (T) and (A_{ct1}) is the corresponding pre-exponential factor (Eq. 1).

Numerical applications require the use of the following convenient simple formulae:

$$(A_{ct}(x_H)/\Omega cm^2) = 4.5266 \times 10^{-6} \cdot x_H^{-17.677}$$

$$R_{ct1}(T)/\Omega cm^2 = 4.5266 \times 10^{-6} e^{\frac{6348.7}{(T/K)}}$$

$$\gamma_g/kJ\,mol^{-1} = 44.745 - 0.14697 \cdot (T/K)$$

$$R_{ct}(x_H)/\Omega cm^2 = 4.5266 \times 10^{-6} e^{\frac{6348.7}{T}} \cdot x_H^{\frac{\gamma_g}{RT}}$$

The values of these coefficients can vary according to the experimental conditions as well as the system characteristics and specificity (Table S2).

We expect that these suggested expressions can be utilized in future estimations for other experimental conditions or other studied materials. We also conclude that the proticity (x_H) of the polyacid (H_xB) has a substantial effect, which can be modeled for future prediction, or estimation and can induce theorists to develop or improve theories[1,16–22,32–37].

Moreover, using linearization technique, we detect another interesting strong correlation between the Arrhenius temperature (T_A) and the compensation temperature (T_{comp}) with the acid proticity (x_H) depicted in Fig. 2.

Linearization technique leads to simple numerical applications requiring the use of the following convenient simple formulas:

$$\frac{1}{T_A - 358} \approx \frac{x_H}{72.71} - \frac{1}{133.21}$$

and

$$\frac{1}{T_{comp} - 223} \approx \frac{x_H}{182.64} - \frac{1}{195.34}$$
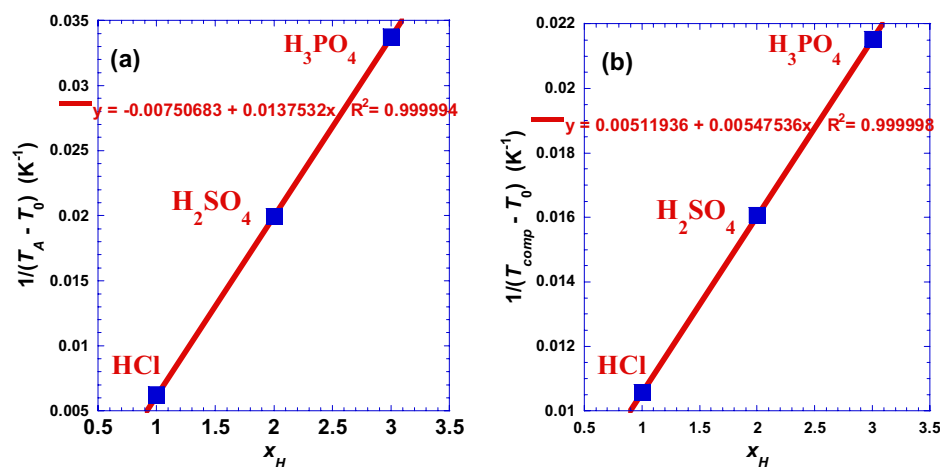

Figure 2. Variation against the acid proticity (x_H) correlation between (**a**): the Arrhenius temperature (T_A) and (**b**): the temperature of compensation (T_{comp}).

where

$$T_{comp} = |\Delta H°/\Delta S°|$$

And the six numerical values are all equivalent to absolute temperatures expressed in Kelvin. We hope that in future works we will find some further interpretations for probable physical significance of the amount of these values, especially for (T_0) indicated in the first member of the two previous equations (Table S3).

Activation energy-temperature dependence

Nevertheless, for the variation of the logarithm of charge transfer resistance ($\ln R_{ct}$) as a function of the inverse of the reciprocal temperature ($1/T$), we have observed feeble net deviations from the linearity of the Arrhenius behavior in some results in literature[1,22,33]. Generally, the linear regression used by the majority of experimenters is just an approximation, because the experimental points are not aligned in practically all researches. For this reason, we consider the slight variation of activation energy with the temperature around the constant values calculated by the classical Arrhenius-type equation, and then the interpretation of the sense of variation against temperature will be very interesting and enrich classical conclusions, discussions and explanations. To differentiate between the classical Arrhenius parameters independent of temperature and those of the new concept, we will name them as current Arrhenius parameters $Ea(T)$ and $\ln A_{ct}(T)$ which are dependent on temperature. So, Eq. 1 is dropped and replaced by a similar expression whose parameters become temperature dependent (Eq. 13).

$$\ln R_{ct} = \ln A_{ct}(T) + \frac{E_a(T)}{R}\left(\frac{1}{T}\right) \tag{13}$$

For that, we propose, as optimization by nonlinear regression, to simply fit the experimental results ($\ln R_{ct}$) with respect of ($1/T$) with only a small-degree polynomial, which can be expressed in its general form as follows:

$$\ln R_{ct} = a_0 + a_1\left(\frac{1}{T}\right) + a_2\left(\frac{1}{T}\right)^2 + a_3\left(\frac{1}{T}\right)^3 + \cdots + a_n\left(\frac{1}{T}\right)^n \tag{14}$$

In fact, in our situation, we are satisfied with two-degree polynomial ($a_3 = 0$, etc.) where results are given in Table 3 [22].

We note that, the mathematical derivation of Eq. 14 can lead us to determine (Ea) and ($\ln R_{ct}$) using the following equations,

$$E_a(T) = R\left(\frac{\partial(\ln R_{ct})}{\partial(1/T)}\right)_P \tag{15}$$

$$\ln A_{ct}(T) = \left(\frac{\partial(T \cdot \ln R_{ct})}{\partial(T)}\right)_P = \ln R_{ct} - \frac{E_a(T)}{RT} \tag{16}$$

$$E_a(T) = [a_1 + 2a_2\left(\frac{1}{T}\right) + 3a_3\left(\frac{1}{T}\right)^2 + \cdots + na_n\left(\frac{1}{T}\right)^{n-1}]R \tag{17}$$

$$\ln A_{ct}(T) = a_0 + 2a_1\left(\frac{1}{T}\right) + 3a_2\left(\frac{1}{T}\right)^2 + 4a_3\left(\frac{1}{T}\right)^3 + \cdots + (n+1)a_n\left(\frac{1}{T}\right)^n \tag{18}$$

In our case, the deviation to the linearity is feeble, so we will consider only a second degree polynomial in our nonlinear regression and consider with excellent approximation that the third coefficient is zero ($a_3 = 0$)[1]. Numerical applications require the use of the following convenient simple formulas:

$$E_a(T)/k\text{Jmol}^{-1} = [a_1 + 2a_2\left(\frac{1}{T}\right)]R/1000$$

$$\ln(A_{ct}(T)/\Omega\text{cm}^2) = a_0 + 2a_1\left(\frac{1}{T}\right) + 3a_2\left(\frac{1}{T}\right)^2$$

Acid	a_0	a_1	a_2	R-square	χ-square
	–	K	K^2	–	–
HCl	38.2266	-2.61907×10^4	5.22150×10^6	0.99929	0.00073
H_2SO_4	19.7075	-1.84969×10^4	4.57233×10^6	0.99987	0.00017
H_3PO_4	-2.1065	-6.78931×10^3	3.06105×10^6	0.99753	0.00153

Table 3. Optimal adjustable coefficients (a_i) from nonlinear regression of Eq. 14.

where we can inject, for each acid, the values of (a_i) from Table 3. The values of these coefficients can vary according to the experimental conditions as well as the system characteristics and specificity.

Results of nonlinear regression are given in Table 4. Figure 3 illustrates this interesting variation of Arrhenius parameters with temperature. We add that we will be forced to augment the polynomial-degree when the general trend of data points, in the plot of $\ln R_{ct} = f(1/T)$ has a strong curvature or a change of curvature (inflection point).

Graphical analysis of (Fig. 3) shows that values of the current Arrhenius parameters $Ea(T)$ and $\ln A_{ct}(T)$ meet those of classical Arrhenius parameters Ea and $\ln A_{ct}$ (Table 4) for practically a unique temperature ($T_{cr} = 320.71$K, 47.56 °C) named as crossover temperature which is approximately equal to the arithmetic mean (319.15K, 46 °C) of the set of five working temperatures indicated in (Table 4). We can notice that this temperature can be an excellent working temperature for our studied system because it gives precise values of Arrhenius parameters whether we treat the data with linear or non-linear regression.

We add that the crossover temperature (T_{cr}) is not specific for the system like the characteristic temperature (τ_0) studied in previous work[1], one must be careful because it cannot be characteristic of the studied system; it is only an intermediate mathematical variable obeying Eq. 19 by simply indicating approximately the temperature of the system during its process. The Eq. 19 can be easily obtained by equalizing Eq. 1 for classical parameters and Eq. 17 for current ones.

$$T_{cr} = \frac{2a_2 R}{E_a - a_1 R} \tag{19}$$

where (Ea) represents the activation energy obtained by linear regression. For numerical applications, we can inject, for each acid, the values of (a_i) from Table 3 and those of (Ea) obtained by linear regression from Table 4. Moreover, we can also use the values of energy parameters determined in our previous work[1] as follows,

$$T_{cr} = \frac{2E_2{}^2}{(E_a + E_1)R} \tag{20}$$

We notice that the middle-temperature ($T_{md} = 323.15$K, 50 °C) of the studied temperature range is very close to the temperature parameter (T_{cr}) as it is shown in Table 4. Indeed, to give an approximate estimation of the mean

T	T	$\ln R_{ct}$	Linear Regression		Non Linear Regression	
			Ea	$\ln A_{ct}$	$Ea(T)$	$\ln A_{ct}(T)$
°C	K	–	kJ mol⁻¹	–	kJ mol⁻¹	–
HCl						
20	293.15	9.6747			78.428	− 22.502
30	303.15	8.6028			68.658	− 18.637
40	313.15	7.8220	52.976	− 12.310	59.511	− 15.034
47.56[a]	320.71[a]	7.3389[c]			52.85[b]	− 12.355[b]
60	333.15	6.7072			42.866	− 8.7680
80	353.15	5.9092			28.105	− 3.6625
			$R^2 = 0.98176$[d]		$\sigma = 0.0260$[e]	$\sigma = 0.0057$[e]
H₂SO₄						
20	293.15	9.8341			105.57	− 33.480
30	303.15	8.4154			97.018	− 30.076
40	313.15	7.2657	83.287	− 24.546	89.009	− 26.920
47.56[a]	320.71[a]	6.5191[c]			83.34[b]	− 24.569[b]
60	333.15	5.4067			74.433	− 21.465
80	353.15	3.9823			61.508	− 16.965
			$R^2 = 0.99440$[d]		$\sigma = 0.0279$[e]	$\sigma = 0.0127$[e]
H₃PO₄						
20	293.15	10.244			117.19	− 37.836
30	303.15	8.9660			111.46	− 35.255
40	313.15	7.4844	102.268	− 31.733	106.10	− 33.265
47.56[a]	320.71[a]	6.5063[c]			102.24[b]	− 31.798[b]
60	333.15	4.9097			96.341	− 29.871
80	353.15	3.2910			87.688	− 26.573
			$R^2 = 0.99589$[d]		$\sigma = 0.0389$[e]	$\sigma = 0.0173$[e]

Table 4. Results of values of the two current Arrhenius parameters $Ea(T)$ and $\ln A_{ct}(T)$ obtained by Eqs. 17 and 18. (a): Crossover temperature T_{cr} (Fig. 3). (b); current Arrhenius parameters $Ea(T)$ and $\ln A_{ct}(T)$ calculated with Eqs. 17 and 18, respectively. (c): logarithm of charge transfer resistance ($\ln R_{ct}$) estimated with Eq. 13. (d): from[22]. (e): Standard deviation σ.
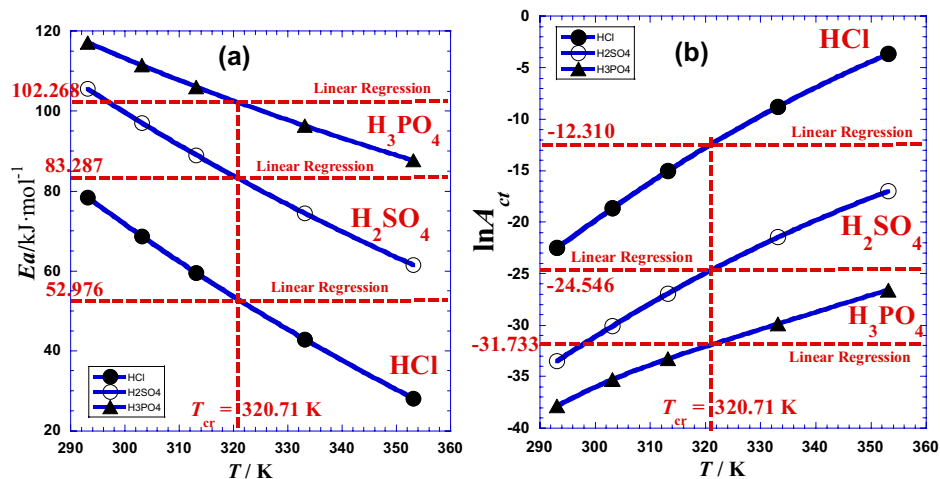
Figure 3. Variation as a function of temperature (T) of, (**a**): the current activation energy Ea (kJ/mol) and (**b**): the logarithm of the current pre-exponential factor ($\ln A_{ct}$) for different acids. (●): HCl; (○): H$_2$SO$_4$; (▲): H$_3$PO$_4$.

activation energy Ea that should be obtained by classical linear regression we can apply the following reasoning. We can calculate the average value of the function $Ea(T)$ expressed by Eq. 17 over a temperature domain $[T_{min}, T_{max}]$ like in our situation $[293.15, 353.15]$K, by the following expression:

$$\overline{E_a} = \frac{1}{T_{max} - T_{min}} \int_{T_{min}}^{T_{max}} E_a(T) dT \tag{21}$$

Which can be adapted for Eq. 21 and can lead to a convenient expression (Eq. 22) for an average value of activation energy without using direct linear regression of $\ln R_{ct}$ with $1/T$.

$$\overline{E_a} = R[a_1 + 2a_2 \frac{\ln\left(\frac{T_{max}}{T_{min}}\right)}{T_{max} - T_{min}}] \tag{22}$$

By similarity to the observed mutual correlation between the two Arrhenius parameters (Ea and $\ln A_{ct}$)[22], likewise we have thought about inspecting the mutual dependence between the two current Arrhenius $Ea(T)$ and $\ln A_{ct}(T)$ by plotting one parameter against the second for the three studied polyacids H$_x$B. In fact, the Fig. 4 shows interesting causal correlation whether for each acid separately or for all three together, for which the quasi-linearity inter-dependence can be expressed as follows:
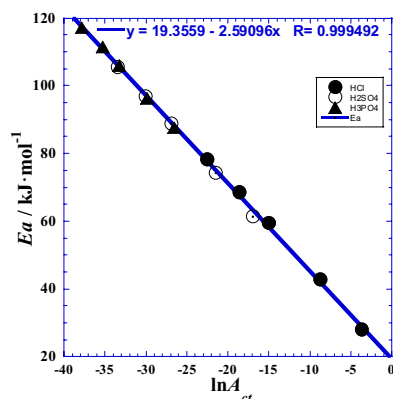
$$Ea(T) = E_{a0} - R\tau_0 \cdot \ln A_{ct}(T) \tag{23}$$

Figure 4. Correlation between the current activation energy Ea (kJ/mol) from polarization and impedance measurements[1] and the current entropic factor of Arrhenius—$R \cdot \ln(A_{ct}/\Omega \text{ cm}^2)/(\text{J K}^{-1} \text{ mol}^{-1})$ for the three acids at atmospheric pressure and separately. (●): HCl, (○): H$_2$SO$_4$, (▲): H$_3$PO$_4$, Solid line: fit in linear regression for both acids.

where E_{a0} (Table 5) is a current activation energy corresponding the zero value of the entropic factor, and the slope τ_0 (Fig. 4) is equivalent to an absolute temperature characteristic of the studied system under such conditions and within the working temperature range.

Hence, some experimenters[1] interpret the sign of the deviation to the Arrhenius linearity as a sub-Arrhenius or super-Arrhenius behaviors. Therefore, we notice that the activation energy Ea (Eqs. 15 and 17) can be interpreted as a potential energy barrier which is assumed to be dependent on temperature $Ea(T)$.

In case of positive values of the activation energy derivative with respect to the reciprocal of absolute temperature at constant pressure: $\left(\frac{\partial E_a(T)}{\partial(1/T)}\right)_P$, super-Arrhenius behavior is observed, whereas for negative values, it is the sub-Arrhenius behavior. For this derivation, the values neighboring zero lead to the classical Arrhenius behavior (Eq. 17) and the a_1-value tends to the classical Arrhenius activation energy Ea, independent of temperature (Table 4).

$$\left(\frac{\partial E_a(T)}{\partial(1/T)}\right)_P = R\left(\frac{\partial^2(\ln R_{ct})}{\partial(1/T)^2}\right)_P = 2a_2 + 6a_3\left(\frac{1}{T}\right) + 12a_4\left(\frac{1}{T}\right)^2 + \cdots + n(n-1)a_n\left(\frac{1}{T}\right)^{n-2} \quad (24)$$

Or else we can write the following:

$$\left(\frac{\partial E_a(T)}{\partial(1/T)}\right)_P = -T^2\left(\frac{\partial E_a(T)}{\partial(T)}\right)_P \quad (25)$$

In our case, the system exhibits a super-Arrhenius behavior, *i.e.* the potential energy barrier is reduced whenever the temperature rises.

Vogel–Fulcher–Tammann model

Generally, in case of clear deviation to the Arrhenius behavior, experimenters try to classify their results in the super-Arrhenius behavior or the sub-Arrhenius one[22] or apply the Vogel–Fulcher–Tammann-type equation (VTF or VFT)[14,23–28] especially when there is divergence of experimental values at low temperature.

However, the variation of the logarithm of charge transfer resistance ($\ln R_{ct}$) against the inverse of the reciprocal temperature ($1/T$) exhibits a feeble deviation from the linearity of the Arrhenius behavior in our previous work (Fig. 1 of[22]) and in some results in literature[26,32–34]. In addition, regarding the suggested pseudo-hyperbolic behavior in previous work[22] where the divergence of the variation of charge transfer resistance (R_{ct}) for low temperatures (Fig. 6 of[22]) exhibits a kind of vertical asymptote, we propose to explore the Vogel–Fulcher–Tammann-type equation (VTF) which is characterized by a vertical asymptote and is used when the test of Arrhenius behavior fails[14,23–28]. In the case of the nonlinear behavior, it is found that the temperature dependence of charge transfer resistance can be physically fitted with the frequently VTF-type equation[14,23–28] expressed as follows:

$$\ln R_{ct} = \ln A_0 + \frac{B_0}{T - T_0} \quad (26)$$

where A_0 and B_0 are optimal constants and T_0 is the Vogel temperature. It's also interesting to use the modified VTF equation which is expressed as follow:

$$\ln R_{ct} = \ln A_0 + \frac{E_0}{R}\left(\frac{1}{T - T_0}\right) \quad (27)$$

where R is the perfect gas constant, E_0 is the VTF activation energy and, A_0 and T_0, are the pre-exponential factor and the Vogel temperature generally comparable to the glass transition temperature in viscosity property[14,23–28]. Experimental data are presented in Table 6 and presented in Fig. 5. For numerical applications, we can inject in Eq. 27, for each acid, the values of (T_0), ($\ln A_0$) and (E_0) from Table 6.

The Eq. 27 shows that when the temperature (T) tends toward (T_0), it implies that the charge transfer resistance (R_{ct}) becomes infinity, which indicates that the corrosion is inhibited. We see that (T_0) decreases whenever the proticity (x_H) of the acid increases (Table 6) while the VTF-energy (E_0), which is in close relation with the activation energy (Ea), varies in the reverse sense.

Acid	E_{a0}	τ_0	τ_0	R-square
	kJ mol^{-1}	K	°C	–
Both acids*	21.64	304.45	31.30	0.99971
HCl	18.952	320.48	47.33	0.99929
H$_2$SO$_4$	16.810	320.48	47.33	0.99931
H$_3$PO$_4$	17.082	320.15	47.00	0.99829
Both acids**	19.356	311.61	38.46	0.99898

Table 5. Optimal parameters (E_{a0} and τ_0), from linear regression of Eq. 23. *Fit in linear regression of (Eq. 23) for classical Arrhenius parameters as independent of temperature[1]. **Fit in nonlinear regression of (Eq. 23) for current Arrhenius parameters dependent on temperature.

Acid	Values of parameters						R-square	SD
	$\ln A_0$	B_0	T_0	T_0	E_0	A_0	R^2	σ
	–	K	K	°C	kJ mol^{-1}	Ω cm^2	–	
HCl	1.294262	492.059	229.45	− 43.70	4.0912	3.6483	0.999906	0.00034
H$_2$SO$_4$	− 6.26592	1695.4	187.80	− 85.35	14.096	0.00190	0.999978	0.00065
H$_3$PO$_4$	− 15.9299	4221.1	132.50	− 140.65	35.096	1.2071×10^{-7}	0.997386	0.00097

Table 6. Optimal coefficients (A_0), Vogel temperature (T_0), the logarithm of pre-exponential factor ($\ln A_0$), VTF activation energy (E_0), R-square (R^2) and standard deviation (σ) for the logarithm of charge transfer resistance ($\ln R_{ct}$) versus absolute temperature in VTF model (Eqs. 26 and 27) for different acids.
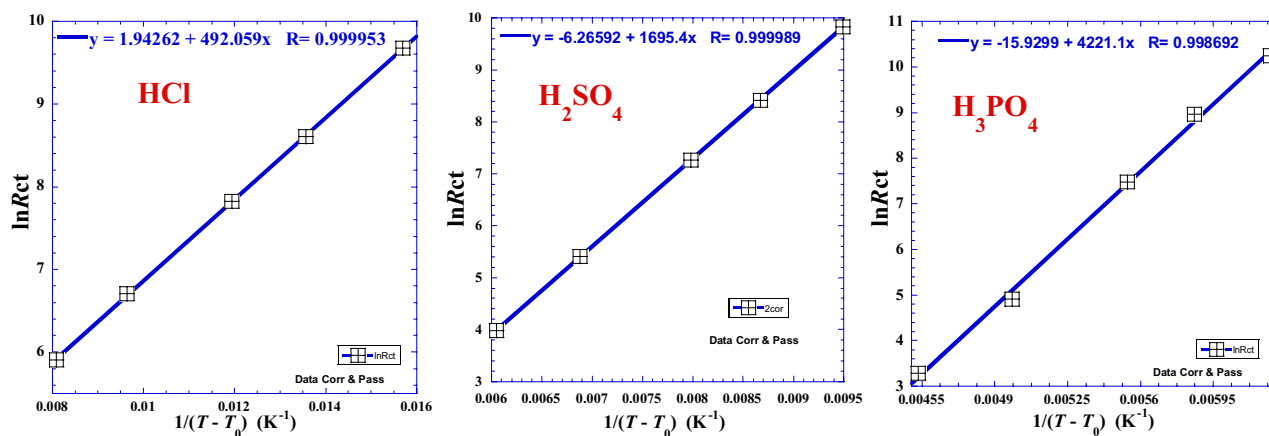
Figure 5. Variation of the logarithm of charge transfer resistance ($\ln R_{ct}$) against $1/(T-T_0)$ for different acids.

Correspondence between the two models

Generally, several experimenters manipulate physical and chemical quantities using various models for comparison and to develop discussions, interpretations and conclusions. This section falls within the scope of the correspondence between the modified Arrhenius equation (Eq. 3) and the VTF model (Eq. 27) to optimize the number of the models commonly utilized for investigations.

When we inject the second member of the VTF expression (Eq. 27) in Eqs. 15 and 16 which are deduced from the principal modified Arrhenius equation (Eq. 2) we can find the new expressions (Eqs. 14 and 15) of the Arrhenius parameters (Ea) and ($\ln A_{ct}$) by comparing term by term without the direct use of the classical Arrhenius-type equation (Eq. 2).

$$E_a(T) = \frac{T^2}{(T - T_0)^2} \cdot E_0 \tag{28}$$

$$\ln A_{ct}(T) = \ln A_0 - \frac{T_0}{R(T - T_0)^2} \cdot E_0 \tag{29}$$

Analyzing the expression of (Eqs. 14 and 15) we can conclude that the two parameters (E_0) and ($\ln A_0$) of the VTF model are simply mathematical intermediary of calculation, except the third one (T_0) which has physical significance indicating that the charge transfer resistance value (R_{ct}) diverges and reaches a very high value when the temperature (T) is very close to (T_0). Moreover, we can say that the non-zero (T_0)-value is the principal cause of the deviation to the linearity of Arrhenius behavior. In fact, we can see in (Eqs. 14 and 15) that when (T_0) tends to zero, the two parameters (E_0) and ($\ln A_0$) become identical to those of Arrhenius (Ea and $\ln A_{ct}$) and in only this situation the two VTF parameters (E_0) and ($\ln A_0$) have a full physical meaning. Furthermore, some theorists state that the Vogel temperature (T_0) is in causal correlation with the corresponding glass transition temperature (T_g)[14,23–28].

Thermodynamic parameters-temperature dependence

Treatments of the free Gibbs energy-temperature dependence considering the corresponding thermodynamic parameters ($\Delta H°$) and ($\Delta S°$) are rarely done in literature[32–34]. The majority consider approximately the constancy of theses parameters and interpret globally the phenomenon governing their studied systems based on their signs (positive or negative), their amounts (high or low values) and not on the eventual slow variation with temperature.

Case of constant thermodynamic parameters

An alternative form of Arrhenius equation is the transition state equation[1,35,38–44]:

$$R_{ct} = \frac{RT}{N_A h} e^{\left(\frac{\Delta H^\circ}{RT} - \frac{\Delta S^\circ}{R}\right)} \tag{30}$$

where (h/J s): is Plank constant, (N_A/mol⁻¹): Avogadro's number, (T/K): absolute temperature, (R_{ct}/Ω m²): charge transfer resistance, (R/J K⁻¹ mol⁻¹): Perfect gas constant (ΔS°/J K⁻¹ mol⁻¹): the entropy of activation and (ΔH°/J mol⁻¹): the enthalpy of activation. Most of experimenters use the following practical expression:

$$\log \frac{R_{ct}}{T} = \log \frac{R}{N_A h} - \frac{\Delta S^\circ}{2.303 R} + \frac{\Delta H^\circ}{2.303 R}\left(\frac{1}{T}\right) \tag{31}$$

where the plot of $\log(R_{ct}/T)$ as a function of $1/T$ gives generally a reliable straight line, with a slope of $+\Delta H^\circ/2.303R$ and an intercept to the ordinate of ($\log R/N_A h - \Delta S^\circ/2.303R$).

However, regarding that the Gibbs free energy of activation (ΔG°) is defined as follows:

$$\Delta G_T^\circ = \Delta H^\circ - T \Delta S^\circ \tag{32}$$

Te determine the two thermodynamic parameters (ΔH°) and (ΔS°), we have to plot the ratio of Gibbs free energy by temperature ($\Delta G^\circ/T$) with the reciprocal of absolute temperature ($1/T$).

Then, regarding the Eq. 32, the Eq. 31 can be reformulated as follows:

$$\Delta G_T^0 = RT \ln \frac{N_A h R_{ct}}{RT} \tag{33}$$

So, the plot of $R \cdot \ln(N_A h R_{ct}/RT)$ as a function of $1/T$ gives a quasi-straight line, with directly a slope of (ΔH°) and an intercept to the ordinate of ($-\Delta S^\circ$). Results are presented in Table 7 and depicted in Fig. 6. The negative values of the Gibbs free energy (ΔG°) indicate that the process of the intermediate complex in the transition

T	T	ΔG°	Linear Regression		Non Linear Regression	
			ΔH°	ΔS°	ΔH°	ΔS°
°C	K	kJ mol⁻¹	kJ mol⁻¹	J K⁻¹ mol⁻¹	kJ mol⁻¹	J K⁻¹mol⁻¹
HCl						
20	293.15	−70.626			80.850	516.72
30	303.15	−75.822			71.176	484.90
40	313.15	−80.440			62.120	455.25
47.55[a]	320.70[a]	−83.766[c]	55.649	432.815	55.649[b]	432.815[b]
60	333.15	−88.837			45.638	403.65
80	353.15	−96.685			31.023	361.63
			$R^2 = 0.98279$[d]		$\sigma = 0.0277$[e]	$\sigma = 0.0213$[e]
H₂SO₄						
20	293.15	−70.238			108.00	608.02
30	303.15	−76.294			99.542	580.03
40	313.15	−81.890			91.620	554.08
47.55[a]	320.70[a]	−86.007[c]	85.959	534.55	85.959[b]	534.55[b]
60	333.15	−92.440			77.203	509.21
80	353.15	−102.34			64.419	472.21
			$R^2 = 0.99458$[d]		$\sigma = 0.0120$[e]	$\sigma = 0.0265$[e]
H₃PO₄						
20	293.15	−69.240			119.61	644.21
30	303.15	−74.907			113.98	623.08
40	313.15	−81.320			108.71	606.82
47.55[a]	320.70[a]	−86.037[c]	104.941	594.307	104.941[b]	594.307[b]
60	333.15	−93.817			99.113	579.11
80	353.15	−104.37			90.606	552.11
			$R^2 = 0.99786$[d]		$\sigma = 0.0057$[e]	$\sigma = 0.0287$[e]

Table 7. Results of values of the two thermodynamic parameters (ΔH°) and (ΔS°) obtained for linear regression by Eqs. 33 and 45 and nonlinear regression (Eqs. 44–49). (a): Crossover temperature T_{cr} (Fig. 11a and b). (b); current thermodynamic parameters $\Delta H^\circ(T)$ and $\Delta S^\circ(T)$ calculated with Eqs. 48 and 49, respectively. (c): Gibbs free energy of activation (ΔG°) estimated with Eq. 44. (d): from[22]. (e): Standard deviation σ.
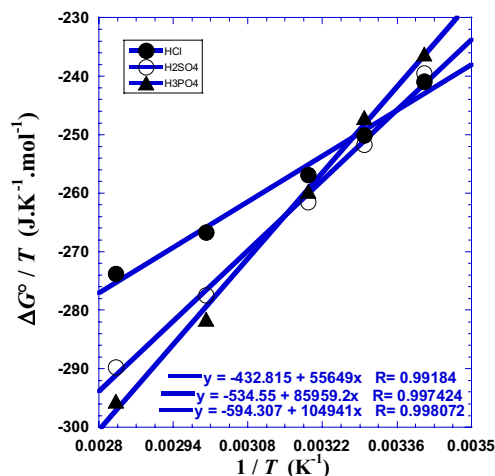
Figure 6. Variation of $\Delta G^*/T$ against the inverse of the absolute temperature ($1/T$) for glassy $Ni_{82.3}Cr_7Fe_3Si_{4.5}B_{3.2}$ alloy corrosion determined from impedance measurements in previous work[1] for the three polyacids HCl, H_2SO_4 and H_3PO_4 at atmospheric pressure. (●): HCl, (○): H_2SO_4, (▲): H_3PO_4. Solid line: linear regression.

state for the corrosion of $Ni_{82.3}Cr_7Fe_3Si_{4.5}B_{3.2}$ alloy in acidic medium is spontaneous, while the positive values of enthalpy ($\Delta H°$) show that the process is endothermic[1,22,30–37].

Effect of protons' number (x_H)

Similarly with our previous work[1,22] for the Arrhenius parameters, we will test the effect of the protons number (x_H) of the polyacids (H_xB). For that, we plotted the two thermodynamic parameters ($\Delta H°$) and ($\Delta S°$) against the logarithm of the acid proticity ($\ln x_H$). Figure 7 shows a linearity, which leads us to wonder if this relationship is valid for other strong acids with same proticity. The slope of the straight line in Fig. 7 represents the enthalpy gap ε_g (Table 8) and it corresponds to the jump of energy value when the proticity increases with unity. The same ascertainment is valid for the Fig. 7 concerning the entropy gap σ_g (Table 8). This observed linearity is similar to the Eqs. 8 and 9 with the same parameters values (Table 2) and it's expressed as follows:

$$\Delta H^°(x_H) = \Delta H^°_1 + \varepsilon_g \cdot \ln x_H \tag{34}$$

$$\Delta S^°(x_H) = \Delta S^°_1 + \sigma_g \cdot \ln x_H \tag{35}$$

where the straight line parameters ($\Delta H°_1$) and ($\Delta S°_1$) correspond to the values of the enthalpy activation and entropy activation related to the monoacid HCl ($x_H = 1$), respectively (Table 8). Numerical applications require the use of the following convenient simple formulas:
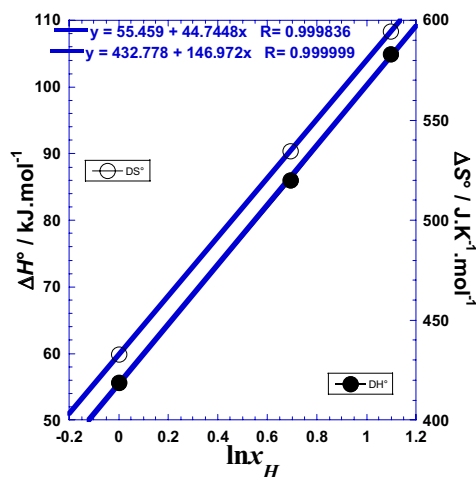

Figure 7. Variation against the logarithm of the acid proticity ($\ln x_H$) of (●): the enthalpy of activation ($\Delta H°/$ kJ mol^{-1}) and (○): the entropy of activation ($\Delta S°/$J K^{-1} mol^{-1}).

ε_g	$\Delta H°_1$	σ_g	$\Delta S°_1$
kJ mol^{-1}	kJ mol^{-1}	J.K^{-1} mol^{-1}	J K^{-1} mol^{-1}
44.745	55.459	146.972	432.778
	55.649*		432.815*

Table 8. Straight lines parameters from linear regression of Eqs. 34 and 35. *Correspond to HCl experimental data, see Table 6.

$$\Delta H^°/\text{kJ mol}^{-1} = 55.459 + 44.745 \cdot \ln x_H$$

$$\Delta S^°/\text{JK}^{-1} \text{mol}^{-1} = 432.778 + 146.972 \cdot \ln x_H$$

We expect that the values of these coefficients can vary according to the experimental conditions as well as the system characteristics and specificity.

However, Eqs. 30, 34 and 35 can be re-expressed to explicit the effect of number of protons (x_H) of the polyacids (H$_x$B) based on monoacid HCl ($x_H = 1$) data.

$$\Delta G^°(x_H) = \Delta G^°_1 + \gamma_g \cdot \ln x_H \tag{36}$$

$$\gamma_g = \varepsilon_g - T \cdot \sigma_g \tag{37}$$

$$\Delta G^°_1 = \Delta H^°_1 - T \cdot \Delta S^°_1 \tag{38}$$

where γ_g represents the free energy gap of acid protonation (*i.e.* when proticity has changed by one unit), $\Delta H°_1$ is the enthalpy of activation related to the monoacid HCl ($x_H = 1$) at given temperature and $\Delta S°_1$ is the entropy of activation. Numerical applications require the use of the following convenient simple formulas:

$$\gamma_g/\text{kJ mol}^{-1} = 44.745 - 0.14697 \cdot (T/\text{K})$$

$$\Delta G^°_1/\text{kJ mol}^{-1} = 55.459 - 0.43278 \cdot (T/\text{K})$$

The values of these coefficients can vary according to experimental conditions as well as the system characteristics and specificity (Tables S1, S2 and S3).

We expect that these suggested expressions can be utilized in future estimations for other experimental conditions or other studied materials. We conclude that the proticity (x_H) of the polyacid (H$_x$B) has a substantial effect, which can be modeled for future prediction, or estimation and can induce theorists to develop or improve theories.

Correlation between the Arrhenius parameters and thermodynamic ones

Analysis of the enthalpy of activation ($\Delta H°$)-values and those of the *Ea*, in the (Fig. 8), shows that the *Ea* and $\Delta H°$ values are very closely related. The same conclusion is also attributed to the correlation between the Arrhenius entropic factor ($-R \cdot \ln As$) and the entropy of activation ($\Delta S°$). Starting from the fact that the values of the two slopes of (Fig. 8) are practically equal to unity (1.00004 and 0.999994), the following expressions are proposed.

$$\Delta H^° = Ea + \delta H^° \tag{39}$$

$$\Delta S^° = -R \cdot \ln A_{ct} + \delta S^° \tag{40}$$

where ($\delta H° = 2.675$ kJ mol^{-1}) and ($\delta S° = 330.46$ J K^{-1} mol^{-1}) are the enthalpy increment and the entropy increment respectively. Numerical applications require the use of the following convenient simple formulae:

$$\Delta H^°/\text{kJ mol}^{-1} = Ea/\text{kJ mol}^{-1} + 2.675$$

$$\Delta S^°/\text{J K}^{-1} \text{mol}^{-1} = -R \cdot \ln(A_{ct}/\Omega \, \text{m}^2)/\text{J K}^{-1} \text{mol}^{-1} + 330.46$$

You have to be careful during discussions, interpretations and comparisons between amount values obtained for (R_{ct}/Ω cm^2) or (R_{ct}/Ω m^2), because the use of CGS or SI systems, which differ in the scale of base units, during the calculations of Arrhenius parameters or thermodynamic ones, doesn't affect the values of the activation energy (*Ea*) and the activation enthalpy ($\Delta H°$), while it gives difference of ($\pm R \cdot \ln 10^4 = \pm 76.579$ J K^{-1} mol^{-1}) when calculating the Arrhenius entropic factor ($-R \cdot \ln A_{ct}$) and the entropy of activation ($\Delta S°$), and this is due to the conversion (cm$^2 \leftrightarrow$ m^2).

We conclude that we can estimate one parameter when the other one is determined by any other technique. We notice that this shift is also due to the fact that the Arrhenius parameters represent the movement between two energy levels related to transition states, while the thermodynamic parameters, as state functions, represent
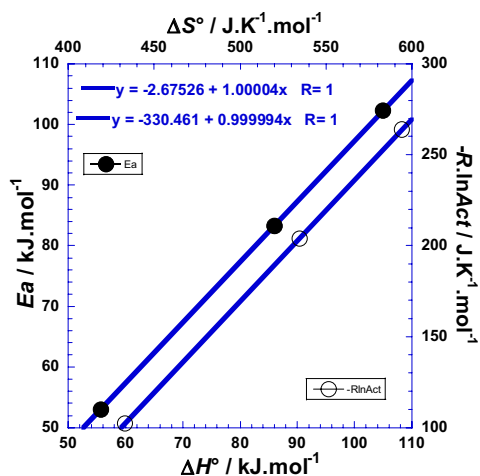
Figure 8. Correlation between the Arrhenius parameters and thermodynamic ones for glassy $Ni_{82.3}Cr_7Fe_3Si_{4.5}B_{3.2}$ alloy. (●):correlation between the enthalpy of activation ($\Delta H°$/kJ mol^{-1}) and the activation energy (Ea/kJ mol^{-1}); (○): correlation between the entropy of activation ($\Delta S°$/J K^{-1} mol^{-1}) and the entropic factor of Arrhenius—$R\cdot\ln(A_{ct}/\Omega$ cm$^2)/($J K^{-1} mol$^{-1})$.

the movement between two energy levels related to equilibrium thermodynamic states[1,22,30–37]. We add that the slopes values of the two straight lines of Fig. 8 are very near to the unity explaining then why that (Ea and $\Delta H°$) and ($-R\cdot\ln A_{ct}$ and $\Delta S°$) have approximately the same value of gap or "jump" (ε_g) and (σ_g) when the number of protons (x) of the acid changes by one unity (Tables 2 and 8). Furthermore, mathematical comparison considering the expressions of Eqs. 1 and 2 and the Eqs. 30–33, which partly include both terms of Eqs. 1 and 2 in each member leads us to expect that the enthalpy increment ($\delta H°$) is in close correlation with the contribution of thermal agitation on the activation enthalpy of the thermal stability related to the spontaneous formation of the hard non-reactive surface of passive film that inhibits the further corrosion (Tables S1, S2 and S3).

Mutual correlation between the thermodynamic parameters

Analysis of the mutual correlation between the enthalpy of activation ($\Delta H°$) and the entropy of activation ($\Delta S°$) represented by the (Fig. 9) shows an excellent linearity which can permit us to estimate the free energy (Eq. 32) with only one thermodynamic parameter ($\Delta H°$) or ($\Delta S°$). This issue is interesting when we can theoretically predict one parameter; we can then deduce the value of the other one by this observed linearity (Tables S1, S2 and S3).

So, the linear enthalpy–entropy dependence observed in Fig. 9 can be expressed as follows,

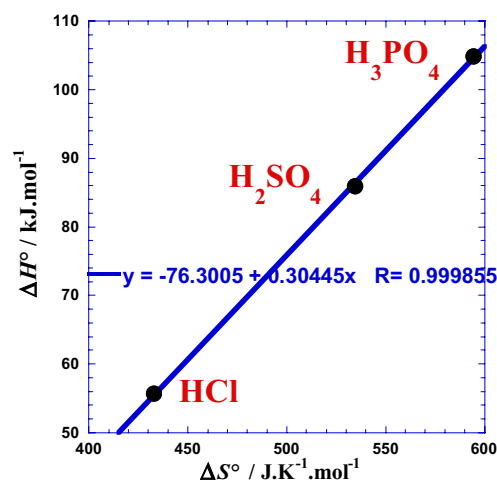$$\Delta H°(T) = \tau_0\big[\Delta S°(T) - \Delta S_c°\big] \tag{41}$$

Figure 9. Mutual correlation between the enthalpy of activation ($\Delta H°$/kJ mol^{-1}) and the entropy of activation ($\Delta S°$/J K^{-1} mol^{-1}) for the three acids HCl, H_2SO_4 and H_3PO_4.

where ($\tau_0 = 304.45$ K) and ($\Delta S^o_c = 250.618$ J K^{-1} mol^{-1}) are the characteristic temperature (Eq. 3) and the characteristic entropy of the studied system at such conditions, respectively. We can consider that the ($\tau_0 \Delta S^o_c$)-product (Eq. 42) is equivalent to a characteristic enthalpy ($\Delta H^o_c = 76.301$ kJ mol^{-1}), the Eq. 41 can be rewritten as follows,

$$\Delta H^o_c = \tau_0 \Delta S^\circ_c \tag{42}$$

$$\Delta H^o(T) = \tau_0 \Delta S^o(T) - \Delta H^o_c \tag{43}$$

Numerical applications require the use of the following convenient simple formulas:

$$\Delta H^\circ(T)/\text{J mol}^{-1} = 304.45 \left[\Delta S^\circ(T) - 250.618 \right]$$

$$\Delta H^\circ(T)/\text{J mol}^{-1} = 304.45 \Delta S^o(T) - 76.301$$

We deduce then, each investigated system has two main specific independent parameters (ΔH^o_c) and (ΔS^o_c), and a dependent parameter (τ_0) which can be simply deduced by the Eq. 42. We note that (ΔS^o_c) corresponds theoretically to the limit of the endothermicity, *i.e.* the activation entropy for which the activation enthalpy becomes zero and changes sign.

Case of temperature-dependent thermodynamic parameters

Almost, all researchers fit thermodynamic behaviors of experimental data in linear regression to conclude about the global thermal character of the studied process (*i.e.* endothermic, etc.). Analyzing the abovementioned study of Arrhenius parameters-temperature dependence, we conclude that is better if we think about the fitting by nonlinear regression to reduce the discrepancy between the straight line and the uncertainty bars of some of experimental scatter points in order to obtain more accurate values of the two thermodynamic parameters (ΔH°) and (ΔS°). Then, the linearity of (ΔG°) with the absolute temperature (T) of Eq. 33 and that of ($\Delta G^\circ/T$) with the reciprocal of absolute temperature ($1/T$) are abandoned and replaced by a polynomial equation with two or three degrees expressed as follows,

$$\frac{\Delta G^0_T}{T} = a_0 + a_1 \left(\frac{1}{T} \right) + a_2 \left(\frac{1}{T} \right)^2 + a_3 \left(\frac{1}{T} \right)^3 + \cdots + a_n \left(\frac{1}{T} \right)^n \tag{44}$$

Given the deviation to the linearity of ($\Delta G^\circ/T$) with the reciprocal of absolute temperature ($1/T$) observed in literature[29–31] is generally not very significant, we judge that we need to consider only a two-degree polynomial fitted in our nonlinear regression (Fig. 10) and acquire excellent approximation where the third coefficient is zero ($a_3 = 0$)[1,22].

The corresponding a_i-coefficients of nonlinear fit are presented in the Table 9. We can clearly see that the statistical quality has improved quite well, and despite this we must pay attention to the fact that this could also be due to the small number of used working temperatures.

The two main thermodynamic parameters, such as the enthalpy (ΔH°) and the entropy (ΔS°) can be determined from the basic thermodynamic Gibbs free energy relationship (Eq. 32).

Te determine values of the two thermodynamic parameters (ΔH°) and (ΔS°), we have to plot the ratio Gibbs free energy by temperature ($\Delta G^\circ/T$) with the reciprocal of absolute temperature ($1/T$). The mathematical handling of Eq. 32 can lead us to determine values of the two thermodynamic constant parameters (ΔH°) and (ΔS°) using
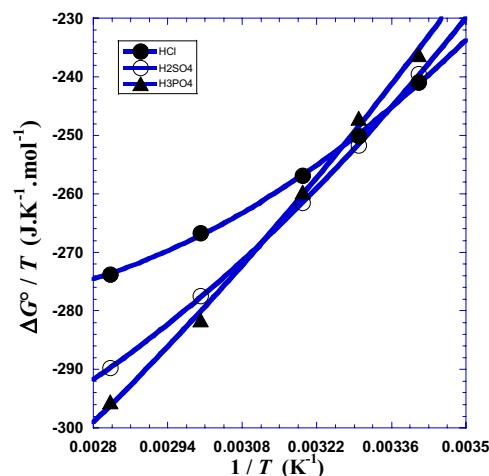

Figure 10. Variation of $\Delta G^*/T$ against the inverse of the absolute temperature ($1/T$) for glassy Ni$_{82.3}$Cr$_7$Fe$_3$Si$_{4.5}$B$_{3.2}$ alloy corrosion for the three polyacids HCl, H$_2$SO$_4$ and H$_3$PO$_4$. (●): HCl, (○): H$_2$SO$_4$, (▲): H$_3$PO$_4$. Curved lines: non linear regression (Eq. 44).

Acid	a_0	a_1	a_2	R-square
	J K⁻¹ mol⁻¹	J mol⁻¹	J K mol⁻¹	–
HCl	− 16.768	− 212,423	4.29865e + 7	0.99935
H_2SO_4	− 170.621	− 148,531	3.76016e + 7	0.99992
H_3PO_4	− 352.116	− 51,109.9	2.50234e + 7	0.99766

Table 9. Optimal a_i-coefficients values obtained by non linear regression for Eq. 44 with second polynomial degree for glassy $Ni_{82.3}Cr_7Fe_3Si_{4.5}B_{3.2}$ alloy corrosion for the three polyacids HCl, H_2SO_4 and H_3PO_4.

the Eq. 45 in the case of linear behavior ($a_2 = 0$ and $a_3 = 0$ in Eq. 44) where the slope value of the straight line is ($\Delta H°$) and intercept on the ordinate is ($-\Delta S°$).

$$\frac{\Delta G_T^0}{T} = \Delta H°\left(\frac{1}{T}\right) - \Delta S° \tag{45}$$

Generally, the two thermodynamic parameters become variable with temperature and mathematical derivation of Eq. 32 can lead us to determine values of the two thermodynamic non-constant parameters $\Delta H°(T)$ and $\Delta S°(T)$ using the following equations.

$$\Delta H°(T) = \left(\frac{\partial(\Delta G°/T)}{\partial(1/T)}\right)_P \tag{46}$$

$$\Delta S°(T) = \frac{\Delta H° - \Delta G_T°}{T} = -\left(\frac{\partial(\Delta G°)}{\partial(T)}\right)_P \tag{47}$$

Application of Eqs. 46 and 47 leads to the general following convenient general expressions.

$$\Delta H^o(T) = a_1 + 2a_2\left(\frac{1}{T}\right) + 3a_3\left(\frac{1}{T}\right)^2 + \cdots + na_n\left(\frac{1}{T}\right)^{n-1} \tag{48}$$

$$\Delta S^o(T) = -a_0 + a_2\left(\frac{1}{T}\right)^2 + 2a_3\left(\frac{1}{T}\right)^3 + \cdots + (n-1)a_n\left(\frac{1}{T}\right)^n \tag{49}$$

Numerical applications require the use of the following convenient simple formulas:

$$\Delta H^o(T)/k Jmol^{-1} = [a_1 + 2a_2\left(\frac{1}{T}\right)]/1000$$

$$\Delta S^o(T)/JK^{-1}mol^{-1} = -a_0 + a_2\left(\frac{1}{T}\right)^2$$

where we can inject, for each acid, the values of (a_i) from Table 9. The values of these coefficients can vary according to the experimental conditions as well as the system characteristics and specificity. Values of the two thermodynamic parameters ($\Delta H°$) and ($\Delta S°$) obtained by linear and nonlinear regressions are presented by Table 7 and depicted in Fig. 11 for the three acids.

Graphical analysis of (Fig. 11) shows that values of the two current thermodynamic parameters $\Delta H°(T)$ and $\Delta S°(T)$ meet those of classical thermodynamic parameters ($\Delta H°$) and ($\Delta S°$) (Table 7) for practically the same unique temperature ($T_{cr} = 320.70K$, 47.55 °C) named as crossover temperature which is approximately equal to the arithmetic mean (319.15 K, 46 °C) of the set of five working temperatures indicated in (Table 7). We can notice that this temperature can be an excellent working temperature for our studied system because it gives precise values of thermodynamic parameters whether we treat the data with linear or with non-linear regression.

We add that the crossover temperature (T_{cr}) is not specific for the system like the characteristic temperature (τ_0) studied in previous work[1], one must be careful because it cannot be characteristic of the studied system; it is only an intermediate mathematical variable obeying Eq. 50 by simply indicating approximately the temperature of the system during its processing. The Eq. 50 can be obtained easily by equalizing Eq. 45 for classical parameters and Eq. 48 for current ones.

$$T_{cr} = \frac{2a_2}{\Delta H° - a_1} \tag{50}$$

where ($\Delta H°$) represents the enthalpy of activation obtained by linear regression (Table 7).

For numerical applications, we can inject, for each acid, the values of (a_i) from Table 9 and those of ($\Delta H°$) obtained by linear regression from Table 7.
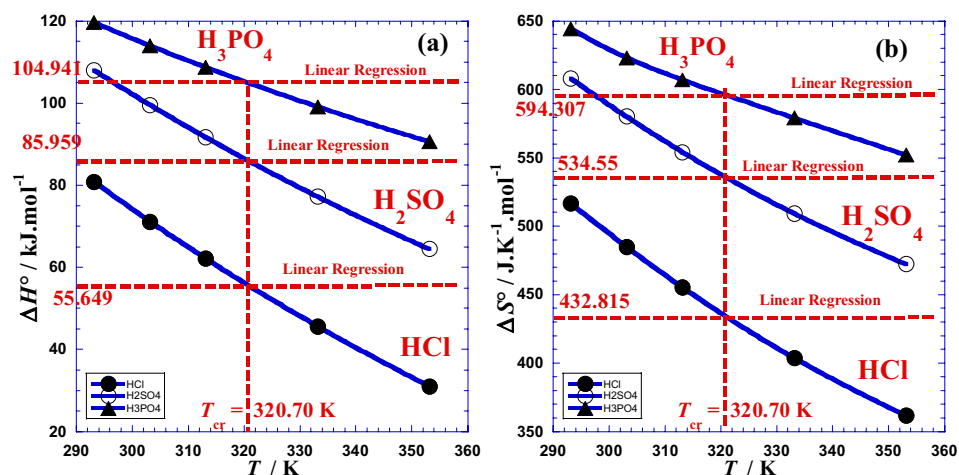
Figure 11. Variation against absolute temperature (T) of (**a**): the enthalpy of activation $\Delta H°(T)$ and (**b**): the entropy of activation $\Delta S°(T)$ for different acids. (●): HCl, (○): H_2SO_4, (▲): H_3PO_4.

We notice that the middle-temperature ($T_{md} = 323.15$K; 50 °C) of the studied temperature range is very close to the temperature parameter (T_{cr}) as it is shown in Table 7. Indeed, to give an approximate estimation of the mean activation enthalpy $\Delta H°$ that should be obtained by classical linear regression we can apply the following reasoning. We can calculate the average value of the function $\Delta H°(T)$ expressed by Eq. 48 over a temperature domain $[T_{min}, T_{max}]$ such as in our situation; [293.15, 353.15]K, by the following expression:

$$\overline{\Delta H°} = \frac{1}{T_{max} - T_{min}} \int_{T_{min}}^{T_{max}} \Delta H°(T) dT \tag{51}$$

Which can be adapted, using Eq. 48, and can lead to a convenient expression (Eq. 52) for an average value of enthalpy of activation without using direct linear regression of $(\Delta G°/T)$ with $1/T$.

$$\overline{\Delta H°} = [a_1 + 2a_2 \frac{ln\left(\frac{T_{max}}{T_{min}}\right)}{T_{max} - T_{min}}] \tag{52}$$

Inspired by to the observed mutual correlation between classical thermodynamic parameters ($\Delta H°$) and ($\Delta S°$) abovementioned, we similarly thought of inspecting their mutual dependence between the two current thermodynamic parameters. $\Delta H°(T)$ and $\Delta S°(T)$ by plotting one parameter against the second for the three studied polyacids H_xB. In fact, the Fig. 12 shows interesting causal correlation, analogous to that of Eq. 43,
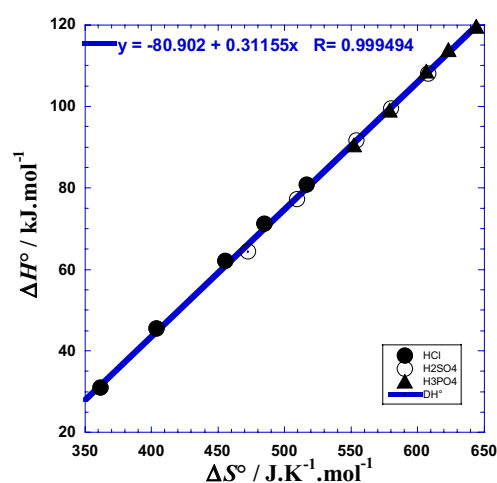

Figure 12. Mutual correlation between the enthalpy of activation ($\Delta H°$/kJ mol^{-1}) and the entropy of activation ($\Delta S°$/J K^{-1} mol^{-1}) for the three acids, both and separately. (●): HCl, (○): H_2SO_4, (▲): H_3PO_4, Solid line: fit in linear regression for both acids.

whether for each acid separately or for all three together, for which the quasi-linearity inter-dependence can be expressed as follows:

$$\Delta H^o(T) = \tau_0 \cdot \Delta S^o(T) - \Delta H_c^o \qquad (53)$$

where ΔH^o_c (Table 10) is a current activation enthalpy corresponding the null value of the activation entropy, and the slope τ_0 (Fig. 12) is equivalent to an absolute temperature characteristic of the studied system at such conditions.

Another advantage, from which we benefit from the dependence on temperature, and other than that of the deduction of the endothermic character of the process, is that which indicates the sense of variation of the enthalpy with the temperature (Table 7) to know if this endothermicity is accentuated or attenuated and thus allowing us to choose the optimal working temperature. The same goes for the discussion and interpretation of entropy. In other words, the dependence with the temperature offers more explanations and fine interpretations than those deduced from only the constancy of thermodynamic parameters.

Conclusion

In one previous work[1], we have studied the effect of the temperature as well as the nature of polyacid medium (HCl, H_2SO_4 and H_3PO_4) on the tendency toward passivation and corrosion resistance for the nickel based glassy $Ni_{82.3}Cr_7Fe_3Si_{4.5}B_{3.2}$ alloy.

In another previous work[22], we have taken into account the deviation to the linearity of the Arrhenius behavior and modeled this particular dependence on temperature. Consequently, we have ended up at the following points. (*i*): The mutual correlation between the Arrhenius parameters, such as, the activation energy determined from polarization and impedance measurements and the entropic factor of Arrhenius permit to reveal a new concept of the current Arrhenius temperature. (*ii*): The causal correlation between the Arrhenius parameters and thermodynamic parameters, permit us to conclude that the activation energy can be considered, with a reliable approximation, as a thermodynamic function. (*iii*): The deviation to the Arrhenius linearity can be classified as a super-Arrhenius behavior for the studied system. (*iv*): The effect of the proton number in polyacid is quantified and modeled. (*v*): The novel suggested model describing a pseudo-hyperbolic behavior gives an excellent agreement (R-square ≈ 1) with the experimental data for each acid separately or for all three together.

As continuation of the abovementioned investigations, we keep on presenting furthermore original modeling of the temperature effect on the thermodynamic parameters as well as the effect of the polyacid proticity. Then, in the present work we extricate the following key points. (*i*): The mutual correlation between the Arrhenius parameters, such as, the activation energy determined from polarization and impedance measurements and the entropic factor of Arrhenius permit to rewrite the Arrhenius-type equation with only one parameter Ea or $\ln A_{ct}$ (Eqs. 5 and 6) and to facilitate, for theorists, to predict the value of one parameter (Eq. 3) when the other one can be predicted by certain theory or approximation. (*ii*): The effect of the proton number (x_H) in polyacid (H_xB) on the two Arrhenius parameters (Ea and $\ln A_{ct}$) is modeled by original expressions (Eqs. 8 and 9) for which we introduce the new concept of the activation energy gap ε_g and the entropic factor gap σ_g permitting to estimate new values of Arrhenius parameter Ea or $\ln A_{ct}$ of a polyacid, using a power law expression (Eqs. 10 and 11), when the same parameter of another acid is available (Table S2). (*iii*): The deviation to the Arrhenius linearity is simply modeled by a polynomial expression (Eq. 14) which reveals the new concept of current Arrhenius parameters depending on temperature (Eqs. 17 and 18) and then permits us to deepen the interpretation and discussion, and add additional elucidations of the effect of temperature on the Arrhenius parameters and the related phenomena governing the studied system. (*iv*): In the same context, we introduce the notion of crossover temperature (Eq. 19) as an optimal working temperature. (*v*): The mutual correlation between the current Arrhenius parameters, depending on temperature, exhibits the same behavior and interdependence whether for each acid separately or for all three together (Eq. 23). (*vi*): We introduced for the first time the Vogel–Fulcher–Tammann-type equation to model the variation of the charge transfer resistance with the respect of temperature (Eq. 27) which shows an excellent agreement with experimental data. (*vii*): In the same context, we have given expressions (Eqs. 28 and 29) permitting to link the VTF parameters and those of the Arrhenius-type equation to facilitate for the users to obtain double results by using only one chosen model. (*viii*): The effect of the proton number (x_H) in polyacid (H_xB) on the two thermodynamic parameters (ΔH^o and ΔS^o) is modeled by satisfying linear expressions (Eqs. 33 and 34) which permit us to estimate the parameters values to one polyacid, knowing those of the monoacid or another polyacid. (*ix*): The correlation between the Arrhenius parameters and the corresponding thermodynamic

Acid	ΔH^o_c	ΔS^o_c	τ_0	τ_0	R-square
	kJ mol⁻¹	J K⁻¹ mol⁻¹	K	°C	–
Both acids*	76.301	250.618	304.45	31.30	0.99971
HCl	84.269	262.947	320.48	47.33	0.99929
H_2SO_4	86.414	269.635	320.49	47.34	0.99931
H_3PO_4	86.028	268.711	320.15	47.00	0.99826
Both acids**	80.902	259.676	311.55	38.40	0.99899

Table 10. Optimal thermodynamic parameters (ΔH^o_c, ΔS^o_c and τ_0), from linear and nonlinear regression of Eqs. 41 and 43. *Fit in linear regression for thermodynamic parameters as independent of temperature. **Fit in nonlinear regression for thermodynamic parameters dependent on temperature.

ones, such as (Ea and $\Delta H°$) and ($-R \cdot \ln As$ and $\Delta S°$), leads us to determine the value of one parameter, simply by a gap (Eqs. 39 and 40) named enthalpy or entropy increment. (*x*): The mutual correlation between the thermodynamic parameters ($\Delta H°$ and $\Delta S°$) shows a linear dependence (Eqs. 41–44) and reveals values of characteristic enthalpy and characteristic entropy, specific to the studied system in such conditions. (*xi*): The feeble deviation to the linearity of ($\Delta G°/T$) *vs.* ($1/T$) permits us to express the dependence of the current thermodynamic parameters $\Delta H°(T)$ and $\Delta S°(T)$ on temperature (Eqs. 48 and 49) and to propose the notion of crossover temperature (Eq. 50) as an optimal working temperature. We conclude that even for the case of the current thermodynamic parameters depending on temperature, the interdependence maintains the linear behavior. (*xii*): we proposed predictive expression form for the charge transfer resistance–temperature dependence to approximately estimate the glass transition temperature (T_g).

After all, it should be mentioned that the previous interpretations made based on the order–disorder or enthalpy–entropy compensation effect could be enhanced by raising the number of working temperatures. Likewise, it cans explain the tendency of these alloys to undergo a disorder-to-order transformation in certain temperature range. We note that some interfaces can introduce an order–disorder transition of this two-dimensional layered network into molecules, leading to increased diffusional characteristics and reduced bonding. Moreover, we can observe an order and disorder combined corrosion morphology of dual-phase Ni-based alloy in the passive state[22,32–37,45–49].

Finally, we must be wary, an interpretation with few experimental data may lead to less certain or unconvincing conclusion.

Data availability
All data generated or analyzed during this study are included in this published article [and its supplementary information files].

References

1. Emran, K. M., Arab, S. T., Al-Turkustani, A. M. & Al-Turaif, H. A. Temperature effect on the corrosion and passivation characterization of $Ni_{82.3}Cr7Fe_5Si_{4.5}B_{3.2}$ alloy in acidic media. *Int. J. Miner. Metall. Mater.* **23**(2), 205–214. https://doi.org/10.1007/s12613-016-1228-x (2016).
2. Liu, J. *et al.* Fast screening of corrosion trends in metallic glasses. *ACS Comb. Sci.* **21**(10), 666–674. https://doi.org/10.1021/acscombsci.9b00073 (2019).
3. Xie, C. *et al.* Corrosion resistance of crystalline and amorphous CuZr alloys in NaCl aqueous environment and effect of corrosion inhibitors. *J. Alloy. Comp.* **879**, 160464. https://doi.org/10.1016/j.jallcom.2021.160464 (2021).
4. Han, J., Nešić, S., Yang, Y. & Brown, B. N. Spontaneous passivation observations during scale formation on mild steel in CO_2 brines. *Electrochim. Acta* **56**(15), 5396–5404. https://doi.org/10.1016/j.electacta.2011.03.053 (2011).
5. Morshed-Behbahani, K. & Zakerin, N. A review on the role of surface nanocrystallization in corrosion of stainless steel. *J. Mater. Res. Technol.* **19**, 1120–1147. https://doi.org/10.1016/j.jmrt.2022.05.094 (2022).
6. Gu, X. *et al.* Corrosion of, and cellular responses to Mg–Zn–Ca bulk metallic glasses. *Biomaterials* **31**(6), 1093–1103. https://doi.org/10.1016/j.biomaterials.2009.11.015 (2010).
7. Li, H. *et al.* Biodegradable Mg–Zn–Ca–Sr bulk metallic glasses with enhanced corrosion performance for biomedical applications. *Mater. Des.* **67**, 9–19. https://doi.org/10.1016/j.matdes.2014.10.085 (2015).
8. Li, Y., Wang, S., Wang, X., Yin, M. & Zhang, W. New FeNiCrMo(P, C, B) high-entropy bulk metallic glasses with unusual thermal stability and corrosion resistance. *J. Mater. Sci. Technol.* **43**(15), 32–39. https://doi.org/10.1016/j.jmst.2020.01.020 (2020).
9. Kiani, F., Wen, C. & Li, Y. Prospects and strategies for magnesium alloys as biodegradable implants from crystalline to bulk metallic glasses and composites—A review. *Acta Biomater.* **103**(1), 1–23. https://doi.org/10.1016/j.actbio.2019.12.023 (2020).
10. Liens, A. *et al.* Effect of alloying elements on the microstructure and corrosion behavior of TiZr-based bulk metallic glasses. *Corros. Sci.* **177**, 108854. https://doi.org/10.1016/j.corsci.2020.108854 (2020).
11. Liu, S., Huang, L., Pang, S.-J. & Zhang, T. Effects of crystallization on corrosion behaviours of a Ni-based bulk metallic glass. *Int. J. Miner. Metal. Mater.* **19**, 146–150. https://doi.org/10.1007/s12613-012-0530-5 (2012).
12. Jindal, R. *et al.* Effect of annealing below the crystallization temperature on the corrosion behavior of Al–Ni–Y metallic glasses. *Corros. Sci.* **84**, 54–65. https://doi.org/10.1016/j.corsci.2014.03.015 (2014).
13. Ma, X. *et al.* Preparation of Ni-based metallic glasses with high corrosion resistance. *J. Non-Cryst. Solids* **443**(1), 91–96. https://doi.org/10.1016/j.jnoncrysol.2016.04.020 (2016).
14. Han, F. *et al.* High temperature oxidation behaviors of Ir-Ni-Ta-(B) metallic glass. *Corros. Sci.* **205**, 110420. https://doi.org/10.1016/j.corsci.2022.110420 (2022).
15. Zhao, K. *et al.* Corrosion behavior of $Ni_{62}Nb_{33}Zr_5$ bulk metallic glasses after annealing and cryogenic treatments. *Chem. Phys. Mater.* **2**(1), 58–68. https://doi.org/10.1016/j.chphma.2022.04.001 (2023).
16. Kim, D.-H. *et al.* Facile enhancement of electrochemical performance of solid-state supercapacitor via atmospheric plasma treatment on PVA-based gel-polymer electrolyte. *Gels* **9**(4), 351. https://doi.org/10.3390/gels9040351 (2023).
17. Wang, D. B. *et al.* Temperature-dependent corrosion behaviour of the amorphous steel in simulated wet storage environment of spent nuclear fuels. *Corros. Sci.* **188**, 109529. https://doi.org/10.1016/j.corsci.2021.109529 (2021).
18. Yang, J. *et al.* Effects of Cr content on the corrosion behavior of porous Ni–Cr–Mo–Cu alloys in H_3PO_4 solution Mat. *Res. Exp.* **8**(9), 096522. https://doi.org/10.1080/1478422X.2021.1927496 (2021).
19. Han, W. & Fang, F. Eco-friendly NaCl-based electrolyte for electropolishing 316L stainless steel. *J. Manuf. Proc.* **58**, 1257–1269. https://doi.org/10.1016/j.jmapro.2020.09.036 (2020).
20. Li, J.-L., Wang, W. & Zhou, C.-g. Oxidation and interdiffusion behavior of a germanium-modified silicide coating on an Nb–Si-based alloy. *Int. J. Miner. Metall. Mater.* **24**, 289–296. https://doi.org/10.1007/s12613-017-1407-4 (2017).
21. Liu, M., Xu, H.-F., Fu, J. & Tian, Y. Conductive and corrosion behaviors of silver-doped carbon-coated stainless steel as PEMFC bipolar plates. *Int. J. Miner. Metall. Mater.* **23**, 844–849. https://doi.org/10.1007/s12613-016-1299-8 (2016).
22. Emran, K., Omar, I. M. A., Arab, S. T. & Ouerfelli, N. On the pseudo-hyperbolic behavior of charge transfer resistance–temperature dependence in corrosion behavior of Nickel based glass alloy. *Sci. Rep.* **12**(6432), 1–12. https://doi.org/10.1038/s41598-022-10462-y (2022).

23. Vogel, H. "Das Temperaturabhaengigkeitsgesetz der Viskositaet von Fluessigkeiten" [The temperature-dependent viscosity law for liquids]. *Phys. Z. (in German)* **22**, 645–646 (1921).
24. Fulcher, G. S. Analysis of recent measurements of the viscosity of glasses. *J. Am. Ceram. Soc.* **8**(6), 339–355. https://doi.org/10.1111/j.1151-2916.1925.tb16731.x (1925).
25. Tammann, G. & Hesse, W. Die Abhängigkeit der Viscosität von der Temperaturbieunterkühlten Flüssigkeiten. [The dependence of viscosity on temperature in supercooled liquids]. *Zeitschriftfüranorganische und allgemeine Chemie (in German)* **156**(1), 245–257. https://doi.org/10.1002/zaac.19261560121 (1926).
26. Cao, C. R. *et al.* Correlation between glass transition temperature and melting temperature in metallic glasses. *Mater. Des.* **60**, 576–579. https://doi.org/10.1016/j.matdes.2014.04.021 (2014).
27. DeRieux, W.-S.W. *et al.* Predicting the glass transition temperature and viscosity of secondary organic material using molecular composition. *Atmos. Chem. Phys.* **18**(9), 6331–6351. https://doi.org/10.5194/acp-18-6331-2018 (2018).
28. Stanciu, I. & Ouerfelli, N. Application Extended Vogel-Tammann-Fulcher Equation for soybean oil. *Orient. J. Chem.* **37**(6), 1287–1294. https://doi.org/10.13005/ojc/370603 (2021).
29. Dallel, M. *et al.* A novel approach of partial derivatives to estimate the boiling temperature via the viscosity Arrhenius behavior in N, N-dimethylformamide + ethanol fluid systems. *Asian J. Chem.* **29**(9), 2038–2050. https://doi.org/10.14233/ajchem.2017.20764 (2017).
30. Dallel, M. *et al.* Prediction of the boiling temperature of 1,2-dimethoxyethane and propylene carbonate through the study of viscosity temperature dependence of corresponding binary liquid mixtures. *Phys. Chem. Liq.* **55**(4), 541–557. https://doi.org/10.1080/00319104.2016.1233181 (2017).
31. Salhi, H. *et al.* Correlation between boiling temperature and viscosity arrhenius activation energy in N, N-dimethylformamide + 2-propanol mixtures at 303.15 to 323.15 K. *Asian J. Chem.* **28**(9), 1972–1984. https://doi.org/10.14233/ajchem.2016.19858 (2016).
32. Ortiz-Oliveros, H. B. *et al.* Modeling of the relationship between the thermodynamic parameters ΔH° and ΔS° with temperature in the removal of Pb ions in aqueous medium: Case study. *Chem. Phys. Lett.* **814**, 140329. https://doi.org/10.1016/j.cplett.2023.140329 (2023).
33. Snoussi, L. *et al.* Thermodynamic parameters modeling of viscous flow activation in ethylene glycol-water fluid systems. *Iran. J. Chem. Chem. Eng.* **39**(3), 287–301. https://doi.org/10.30492/ijcce.2020.34707 (2020).
34. Alakhras, F., Al-Abbad, E., Alzamel, N. O., Abouzeid, F. M. & Ouerfelli, N. Contribution to modeling the effect of temperature on removal of nickel ions by adsorption on nano-bentonite. *Asian J. Chem.* **30**(5), 1147–1156. https://doi.org/10.14233/ajchem.2018.21252 (2018).
35. Arab, S. T. & Al-Mhyawi, S. R. Effect of temperature on the corrosion inhibition on mild steel in 2.0 M H_2SO_4 by some organic compounds containing S and N atoms in absence and presence of halides. *Orient. J. Chem.* **24**(2), 365–380 (2008).
36. Mu'azu, N. D. *et al.* Inhibition of low carbon steel corrosion by a cationic Gemini surfactant in 10wt.% H_2SO_4 and 15wt.% HCl under static condition and hydrodynamic flow. *S. Afr. J. Chem. Eng.* **43**(232), 244. https://doi.org/10.1016/j.sajce.2022.10.006 (2023).
37. Haladu, S. A. *et al.* Inhibition of mild steel corrosion in 1 M H_2SO_4 by a gemini surfactant 1,6-hexyldiyl-bis-(dimethyldodecylammonium bromide): ANN, RSM predictive modeling, quantum chemical and MD simulation studies. *J. Mol. Liq.* **350**, 118533. https://doi.org/10.1016/j.molliq.2022.118533 (2022).
38. Putilova, I. N. *Metallic Corrosion Inhibitors* (Pergamon Press, 1960).
39. Hundson, R. M., Butler, T. J. & Warring, C. J. The effect of pyrrole-halide mixtures in inhibiting the dissolution of low-carbon steel in sulphuric acid. *Corros. Sci.* **17**(7), 571–581. https://doi.org/10.1016/S0010-938X(77)80003-6 (1977).
40. Putilova, I. N., Balezin, S. A. & Barannik, V. P. in H. E. Bishop (Ed) Metallic Corrosion Inhibitors. 27 (Pergamon, 1960).
41. Hoar, T. P. & Holliday, R. D. The inhibition by quinolines and thioureas of the acid dissolution of mild steel. *J. Appl. Chem.* **3**(11), 502–513. https://doi.org/10.1002/jctb.5010031105 (1953).
42. Khalil, M. W., Abdou, M. S. A. & Ammar, I. A. Corrosion of mild steel in acid solutions containing thiourea and thiosemicarbazide. *Mat. Sci. Eng. Technol.* **21**(6), 230–235. https://doi.org/10.1002/mawe.19900210608 (1990).
43. Abd El-Nabey, B. A., El-Awady, A. A. & Aziz, S. G. Structural effects and mechanism of the inhibition of acid corrosion of steel by some dithiocarbamate derivatives. *Corros. Prev. Control* **38**(3), 68–74 (1991).
44. Fouda, A. S., El-Kaabi, S. S. & Mohamed, A. K. Substituted phenyl n-phenylcarbamates as corrosion inhibitors for iron in hydrochloric acid. *Anti-Corros. Methods Mater.* **36**(8), 9–12. https://doi.org/10.1108/eb020787 (1989).
45. Fan, Y., Cao, P., Iwashita, T. & Ding, J. Modeling of structural and chemical disorders: From metallic glasses to high entropy alloys. *Front. Mater.* **9**, 1006726. https://doi.org/10.3389/fmats.2022.1006726 (2022).
46. Guttman, L. Order-disorder phenomena in metals. *Solid State Phys.* **3**, 145–223. https://doi.org/10.1016/S0081-1947(08)60133-2 (1956).
47. Lei, X. *et al.* Investigation of the ordered and disordered corrosion morphologies on Ni-based alloy in the passive state. *Corros. Sci.* **224**, 111490. https://doi.org/10.1016/j.corsci.2023.111490 (2023).
48. Dideriksen, K. *et al.* Order and disorder in layered double hydroxides: Lessons learned from the green Rust Sulfate-Nikischerite Series. *ACS Earth Space Chem.* **6**(2), 322–332. https://doi.org/10.1021/acsearthspacechem.1c00293 (2022).
49. Tawancy, H. M. Enhancing the corrosion resistance of near-stoichiometric Ni_4Mo alloy by doping with yttrium. *Metallogr. Microstruct. Anal.* **1**, 99–105. https://doi.org/10.1007/s13632-012-0018-8 (2012).

Author contributions

N.O., conceived of the presented idea and planned and carried out the simulation. Also he developed the theory and performed the computations. Khadijah M. Emran, worked out almost all of the technical details on the the original work [ref. 1, K.M. Emran, S.T. Arab, A.M. Al-Turkustani, H.A. Al-Turaif. Temperature effect on the corrosion and passivation characterization of Ni82.3Cr7Fe3Si4.5B3.2 alloy in acidic media. International Journal of Minerals, Metallurgy and Materials 23(2);2016:205-214. https://doi.org/10.1007/s12613-016-1228-x All authors discussed the results and contributed to the final manuscript. they also ,took the lead in writing the manuscript and provided critical feedback and helped shape the research, analysis and manuscrip. Regarding the data availability statement "Please include the Data Availability statement in the manuscript (before references under separate heading). " "The datasets used and/or analysed during the current study available from the corresponding author on reasonable request."

Competing interests

The authors declare no competing interests.

Additional information